Computational and Theoretical Chemistry 1070 (2015) 117–125

Contents lists available at ScienceDirect

Computational and Theoretical Chemistry

journal homepage: www.elsevier.com/locate/comptc

Interaction of LD14 and TiO_2 in dye-sensitized solar-cells (DSSC): A density functional theory study

Fernando Mendizabal [a,b,*], Alfredo Lopéz [a,c], Ramiro Arratia-Pérez [b,d], Gerald Zapata-Torres [e]

[a] Departmento de Química, Facultad de Ciencias, Universidad de Chile, P.O. Box 653, Las Palmeras 3425, Ñuñoa, Santiago, Chile
[b] Millennium Nucleus of "Molecular Engineering for Catalysis and Biosensors", ICM, Chile
[c] Departamento de Química, Facultad de Ciencias Básicas, Universidad Metropolitana de Ciencias de la Educación, Casilla 147, Santiago, Chile
[d] Doctorado en Fisicoquímica Molecular, Relativistic Molecular Physics (ReMoPh) Group, Universidad Andrés Bello, República 275, Santiago, Chile
[e] Departamento de Química Inorgánica y Analítica, Facultad de Ciencias Químicas y Farmacéuticas, Universidad de Chile, Casilla 233, Santiago 1, Chile

ARTICLE INFO

Article history:
Received 8 June 2015
Received in revised form 4 August 2015
Accepted 4 August 2015
Available online 10 August 2015

Keywords:
$LD14–TiO_2$ model
Coordination energies
Absorption spectrum
TDDFT

ABSTRACT

The interaction and electron injection processes of the LD14 dye on TiO_2 cluster (anatase phase) in dye-sensitized solar cells (DSSCs) have been studied through calculations based on density functional theory (DFT) at the B3LYP, PBE and TPSS levels along with dispersion effects. The interaction of the LD14 dye with the TiO_2 clusters was quantified using the DFT-D3 levels. The TDDFT calculations with the B3LYP-D3 in phase solvent (THF) in the LD14 and LD14–TiO_2 models are the most suitable for describing the observed absorption energy bands. The free energy changes for electron injection support the better performance of LD14 on the TiO_2 clusters.

1. Introduction

Since several decades scientific studies have been focused on the energy problems that human activity is confronting. Nowadays, energy consumption is about 15 TW, and it is expected that it will increase by a factor of two in the coming decades [1]. Development of renewable, low cost, environmental friendly and sustainable energy is one of the major energy issues of the current era. From the different energy alternatives that have been explored and developed, the solar energy is one of the most promising since it is an important sustainable energy source in the present and the near future; even though a variety of energy sources have to be explore yet, at least until the new techniques of solar-energy capturing devices are mature enough to replace the older energy sources [2]. As a matter of fact only 0.02% of the solar radiation requires to be captured to satisfy future energy needs. Many different principles have been proposed for constructing efficient solar-energy capturing devices. Thus, in the last two decades, dye-sensitized solar cells (DSSCs) have attracted much attention, and attempts are being made so far to get these new devices to replace commercial solar cells made with silicon [3,4]. Nevertheless, they have high production and maintenance costs, leading to a continuous search for replacements. DSSCs were proposed for the first time by Grätzel et al. [5,6].

The chemical and physical processes of the Grätzel cells are now largely known, while the details at the molecular level are less elucidated. So, to improve the efficiency of the dye-sensitized solar cells it is necessary to find a suitable molecular called "dye" for the light capturing process. The most important Grätzel's DSSCs are based on the adsorption of metallic complexes (e.g. ruthenium and zinc) on nanocrystalline titanium dioxide films [4,7–10]. Among the studied compounds, ruthenium(II)bipyridyl (N3, N719 and N749) complexes have proved to be the more efficient TiO_2 sensitizers [7–14]. This efficiency is measured by the power conversion index (η) and Grätzel cells based on the sensitization of TiO_2 by molecular dyes have a η among 7–11%. This efficiency makes applications feasible; however, ruthenium is an expensive metal, thus novel dyes are desirable for highly efficient DSSCs [4]. Recently, it is possible to identify in the literature other inorganic solar cells that are alternative to ruthenium complexes such as large π–π aromatic molecules zinc porphyrins (ZnP) [15–21]. These highly efficient DSSCs have good properties of photostability, light-harvesting capabilities, and low-cost. The central metal is zinc and η is about 6–7%. Among the most efficient Zn systems it is possible to find YD2, YD2-o-C8, ZnPBAT, LD13 and LD14 [22,23].

We focus our attention on solar cells based on ZnP. All zinc porphyrin based sensitizers with antenna molecules as the ones described above have been designed and applied to DSSC. These

* Corresponding author at: Departmento de Química, Facultad de Ciencias, Universidad de Chile, P.O. Box 653, Las Palmeras 3425, Ñuñoa, Santiago, Chile.
E-mail address: hagua@uchile.cl (F. Mendizabal).

http://dx.doi.org/10.1016/j.comptc.2015.08.005
2210-271X/

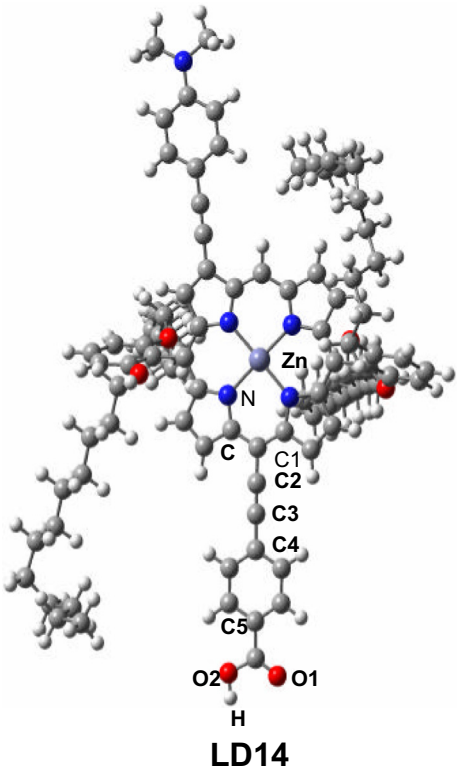

Fig. 1. LD14 dye sensitizer model.

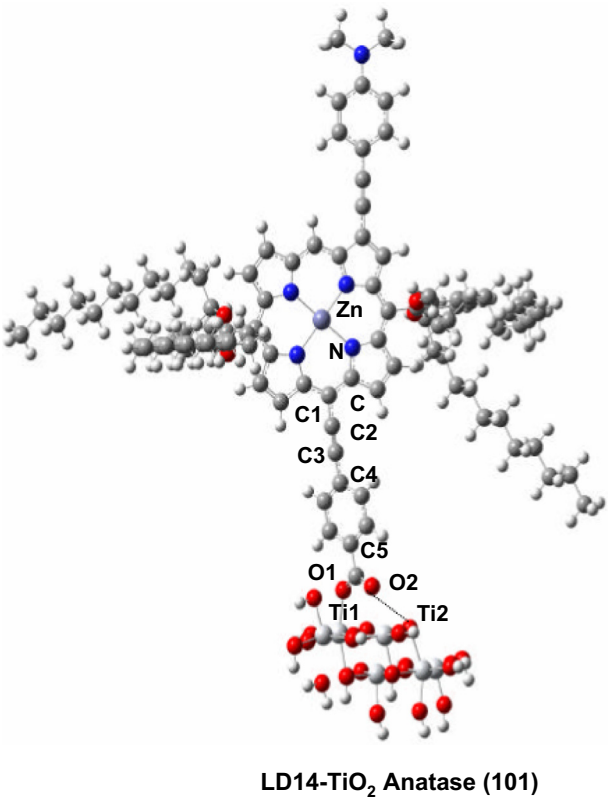

Fig. 2. LD14 on TiO_2 dye model.

systems show metallo-supramolecular interactions, enhancing their light-harvesting efficiency. Optimization of the devices performance for the push–pull zinc macrocycles have high power conversion efficiency. Among the different systems studied experimentally, it is possible to find the dye assigned as LD14. The LD14 system has a $\eta = 10\%$, opening a new field using porphyrin-based DSSC [24]. The high performance of LD14 is due to the introduction of ortho-alkoxylated phenyl aromatic groups in the meso-position of the porphyrin ring. In general, these groups are donor–acceptor (D–A) substituents with promising photovoltaic properties [25–28].

In this context, previous systems have shown an arrangement in a single supramolecular assembly able to absorb a large portion of the solar spectrum in the region between the visible and the near-IR. In several studies it has been mentioned that the use of supramolecular interactions in solar cells is scarce [25–28]. Solar energy conversion efficiency (η) in photoelectrochemical cells is a function of several factors such as: the collection of electrons by the external circuit, the electron injection quantum yield (i.e., the ratio of injected electrons to absorbed photons), and the absorbance (the ratio of absorbed photons to incident photons) [10,11]. Dyes that support efficient intramolecular energy transfer (i.e., the antenna effect) can be designed to display broader absorption bands and/or absorption bands with high extinction molar coefficients [15–21]. Electron injection quantum yields, on the other hand, depend on the dye's excited state and the relative position of the conduction band edge of titanium dioxide. The properties of the excited state can be modulated by the appropriate selection of ligands and/or peripheral substituents, while the conduction band edge of titanium dioxide can be selected by the acid-base pretreatment of the TiO_2 films or through the addition of potential determining cations to the external bath.

An important aspect regarding DSSCs corresponds to the interaction between the dye sensitizer and the TiO_2. Usually the sensitizer molecules have a carboxyl group that interacts with the solid electrode. It is of fundamental importance the determination of the geometric structure of the adsorbed dye state and the electronic coupling with the Ti(3d) conduction band. Over the past five years a number of theoretical studies at the quantum chemical (density functional theory) and molecular dynamics levels of solar cells with ruthenium complexes have been published [12–15,29–34]. These studies have modeled the interaction of the ruthenium sensitizers with the (101) plane of TiO_2 (anatase) or nanocluster of TiO_2. The theoretical results show that the dye is attached via carboxylate groups.

The aim of this work is to extend the idea to supramolecular systems using the well-known coordination preference of the LD14 dye. The design of supramolecular interactions using solar cells is still insufficient. In nature, it is possible to find supramolecular antenna complexes that harvest light [24]. The chemical bonding between the TiO_2 surface and the dye needs to be completely understood. We propose here to carry out a theoretical study to find out which anchor groups would produce improved conjugation within these macrocycle rings. The largest molecular systems that can be tackled with high reliability using state of the art quantum chemistry methods are about the same size as the light-receptor system of the Grätzel cells [25–28]. The model systems considered in the calculations consist of a dye attached to a TiO_2 cluster representing the TiO_2 surface [29–34]. Theoretical models including optimizations of the molecular structures can be used to identify and characterize suitable light-capturing molecules. Ground-state calculations show how the dye binds to TiO_2. Single-point quantum chemical calculations of the excited-states provide excitation energies, information about the vertical excitation processes, and properties of the exciton as well. The light-absorption process in dye-sensitized solar cells will be studied using time-dependent density functional theory (TDDFT). Determining the kind of interaction between LD14 and TiO_2 will

allow for a better understanding of the complete mechanism involved in solar cells and of in the design of future systems.

2. Models and computational details

The LD14 model used in this study is depicted in Fig. 1. C_1 symmetry was adopted for the protonated dye. The geometry of LD14 in the ground state was fully optimized at the B3LYP, PBE and TPSS levels in gas and solvent (THF: tetrahydrofuran) phases. This was carried out because we are interested in studying the formation of supramolecular systems, where the coordination interactions are important. Grimme's dispersion correction was used for those functionals whenever available, and their use is indicated by appending "DFT-D3" to the acronym of the density functional [35,36].

The fully relaxed structure of the LD14 dye adsorbed on the TiO_2 surface obtained is shown in (Fig. 2). The structure of TiO_2 is kept fixed. For the LD14-TiO_2 interaction model (C_1 symmetry) we used two approaches. The first considered the dye molecule without a proton in the —COOH group; this effect is consistent with experimental and theoretical studies with different porphyrins when carboxylic acid is bound to the TiO_2 surface by means of mono- and bidentate bridging modes. Depending on the dye it is possible to find mono- or bidentate coordination [37–40]. With respect to the COO^- group, it is experimentally established that the IR spectra exhibit a significant increase of the symmetric carboxylate band at around 1400 cm^{-1} [23]. The disappearance of the C=O frequency confirms that the proton is detached from the carboxylic acid group during porphyrin adsorption on TiO_2. This situation has been studied and tested using theoretical models. The second approach is the choice of the TiO_2 surface model. In the literature there are many models of various shapes and sizes from Ti_5 to Ti_{80} [8,9]. Small scale theoretical models of TiO_2 that have been used to study the interaction of different dyes (N749, N3, C101, J3, etc.) giving reasonable results [41,42]. In the present work the $[Ti_6O_{21}H_{18}]$ model was cut from crystal structures of anatase to simulate the surface of TiO_2. Hydrogen atoms were used to saturate the covalent bonds of the O atoms.

The excitation energies were obtained at the DFT level by means of the time-dependent perturbation theory approach (TD-DFT) [43–45]. The excitation spectrum was simulated from the optimized geometry of the theoretical model. The TD-DFT calculations do not evaluate the spin–orbit coupling, and the values are averaged. Moreover, we have used the AOFORCE module [46] implemented in Turbomole [47] to estimate the vibration frequency of the —COOH group in LD14 free and —COO^- group attached to TiO_2. The polarizable continuum model (PCM) was used to simulate the THF solvent effects from the COSMOS program [48]. In addition, the counterpoise correction for the basis-set superposition error (BSSE) was used for the calculated interaction energies between LD14 and TiO_2.

The calculations were done using the Turbomole package (version 6.5) [47]. For Zn and Ti, the 10 valence-electron (VE) pseudopotential (PP) of Andrae et al. [49] was employed. We used two *d*-type polarization functions on Zn and Ti [50]. Also, the C, N and O were treated through PPs, using double-zeta basis sets with the addition of one *d*-type polarization function [51]. For the H atom, a double-zeta basis set plus one *p*-type polarization function was used [52]. The basis sets were taken as Zn (6s5p3d|8s7p6d), Ti (6s5p3d|8s7p6d), O (2s2p1d|4s4p1d), C (2s2p1d|4s4p1d), N (2s2p1d|4s4p1d), and H (2s1p|4s1p). All geometry calculations were obtained using the efficient resolution of identity (RI) [53].

Table 1
Main geometric parameters of the LD14 ligand with different methods including gas and solvent effect (solv). Distances in pm and angles in degrees.

Method	Zn—N	N—C	C—C1	ZnNCC1°	C2—C3	NCC1C2°	C5—O1	C5—O2	O2C5O1°
B3LYP	204.6	137.8	141.1	4.0	121.8	178.1	123.5	138.5	121.0
TPSS	204.9	138.9	141.9	4.1	122.8	178.0	124.5	139.8	121.0
PBE	205.2	138.5	141.8	3.2	123.0	178.4	124.4	139.4	121.1
B3LYP-D3	204.3	137.6	140.6	2.7	121.5	178.2	123.2	138.1	121.0
TPSS-D3	204.9	138.4	141.6	2.8	122.5	178.9	124.1	139.3	121.0
PBE-D3	204.9	138.2	141.1	2.8	122.5	178.9	123.9	139.3	121.1
B3LYP (solv)	204.8	138.0	141.3	4.1	121.8	178.6	123.6	138.4	121.2
TPSS (solv)	205.1	139.1	142.0	4.4	122.7	178.5	124.6	139.5	121.1
PBE (solv)	205.3	138.7	141.9	3.3	123.2	178.7	124.8	139.5	121.4
B3LYP-D3 (solv)	204.9	137.5	141.0	2.5	121.6	178.5	123.8	137.1	120.5
TPSS-D3 (solv)	205.0	138.1	141.1	2.8	122.1	178.2	124.5	139.3	121.1
PBE-D3 (solv)	205.2	138.3	141.5	2.9	123.4	178.3	124.5	137.8	121.2

Table 2
Main geometric parameters of the LD14–[TiO_2] with different methods including gas and solvent effect (solv). Distances in pm and angles in degrees.

Method	Zn—N	N—C	ZnNCC2°	NCC1C2°	Ti1—O1	Ti2—O2	C5—O2	C5—O1	O2C5O1°	Ti1O1C5°
B3LYP	204.6	138.5	1.5°	178.1°	208.3	243.6	130.9	127.5	129.1°	136.6°
TPSS	204.9	139.3	1.7°	177.7°	209.1	234.4	128.7	131.7	129.9°	136.0°
PBE	206.5	137.4	1.4°	178.2°	209.6	240.8	128.4	131.5	129.7°	135.9°
B3LYP-D3	204.5	138.4	1.2°	178.9°	207.9	243.2	130.3	127.4	130.1°	136.7°
TPSS-D3	204.9	139.3	0.6°	178.6°	208.6	233.2	128.8	131.6	132.2°	136.1°
PBE-D3	204.9	139.0	2.6°	177.4°	209.4	238.9	128.5	131.5	129.8°	136.0°
B3LYP (solv)	204.7	138.7	2.3°	179.1°	208.1	254.8	127.7	131.5	127.5°	137.1°
TPSS (solv)	205.1	139.5	1.5°	178.1°	209.0	236.3	127.8	132.5	128.5°	136.5°
PBE (solv)	206.3	137.6	1.3°	178.6°	209.3	245.5	127.9	132.1	128.3°	136.3°
B3LYP-D3 (solv)	204.6	138.5	2.0°	179.0°	208.0	245.5	127.5	131.1	127.4°	136.9°
TPSS-D3 (solv)	204.7	139.3	0.6°	178.6°	208.6	233.2	128.8	131.6	132.2°	136.1°
PBE-D3 (solv)	205.8	137.5	1.1°	178.2°	208.8	242.3	127.2	131.8	127.6°	136.2°

3. Results and discussion

3.1. Geometric structures and YD2–TiO_2 coordination energy

The optimized geometry of LD14 at the different levels is shown in Fig. 1. LD14 is composed of different functional groups: ortho-alkoxylated phenyl aromatic groups in the meso-position of the porphyrin ring acting as an electron donor, the phenylethynyl group as part of the bridge, the carboxylic acid moiety as an acceptor, and the porphyrin chromophore as the π-bridge in this particular donor π-conjugate-bridge acceptor (D-π-A) structure. The selected geometrical parameters are listed in Table 1. The bond lengths, bond angles and dihedrals are very similar at the different levels and phases (gas and solvent). The inclusion of the dispersion term at the D3 did not produce major changes.

We linked LD14 with the TiO_2 model (see Fig. 2) through the carboxylate moiety on the Ti atoms of the (101) plane. The LD14 was then fully optimized in its ground state, and the main parameters are shown in Table 2. It can be seen that the structural parameters change from free LD14 to LD14-TiO_2. When LD14 is coordinated with TiO_2, LD14 does not suffer major changes. The most relevant changes in the geometry remain on the carboxylate group which acts as a bidentate ligand with TiO_2. According to our calculations, the O1 and Ti1 bonds are between 208 and 209 pm depending on the method and the medium used. In general, there is not a very large variation of this Ti—O distance. The second distance, Ti2—O2, is longer (between 234 and 255 pm) and keeps a lightly bidentate character. The Ti—O distances are slightly shorter when the dispersion effects (D3) and a solvent medium are used in the calculations. The C5—O2 and C5—O1 distances and the O2C5O1 angle adopt a more relaxed geometry than when LD14 is free.

Also, we have estimated the vibrational frequencies for the LD14 dye when it is free and coordinated with the TiO_2 clusters. These results have been obtained at the B3LYP-D3 level in the gas phase. In particular, we focus on the vibration frequency of the —COO^- group. For the free dye a vibration frequency of 1665 cm^{-1} is obtained, which is closer to the reported experimental value of 1700 cm^{-1} [23]. On the other hand, when LD14 is linked with TiO_2, the vibration frequency decreases to 1345 cm^{-1}, which is again closer to the experimental reported value of 1400 cm^{-1}. This is a clear evidence of the coordination effects of the —COO^- group on the TiO_2 electrode via the $2\pi^*$ COO^- orbitals. These results are very close to the reported LD14–TiO_2 system.

We have estimated the LD14–TiO_2 intermolecular interaction energies for the proposed model with and without counterpoise correction (CP) for the basis-set superposition error (BSSE), and the results are shown in Table 3. The model produces a coordinated bond at all levels. When the results between DFT and DFT-D3 with CP are compared, it can be noticed that the interaction energy is stabilized between 8.0 and 5.0 kcal mol^{-1}. However, the interaction energies without CP are strongly overestimated at all levels. When solvent effects are introduced, it is seen that the interaction energy decreases slightly with CP. However, with CP and the solvent effects the interaction energy is not overestimated. Clearly, at this level there are error compensation effects. The magnitudes reported here are in the same range as those for similar systems

Table 3
Intermolecular interaction energies, ΔE_{int} (kcal mol^{-1}) between TiO_2 ($[Ti_6O_{21}H_{18}]$) and LD14 with and without counterpoise correction (CP).

Method	ΔE_{int} [a]	ΔE_{int} [b]
B3LYP	−42.7	−58.7
TPSS	−41.9	−55.7
PBE	−39.5	−54.0
B3LYP-D3	−51.6	−67.3
TPSS-D3	−49.2	−62.7
PBE-D3	−45.1	−59.6
B3LYP (solv)	−39.8	−42.7
TPSS (solv)	−41.5	−41.8
PBE (solv)	−40.1	−40.4
B3LYP-D3 (solv)	−43.1	−45.4
TPSS-D3 (solv)	−48.3	−48.8
PBE-D3 (solv)	−45.4	−45.3

[a] With CP.
[b] Without CP.

Table 4
Natural Population Analysis (NPA) charge for the —CO_2^- group in LD14 attached to TiO_2, with both systems free in the gas and solvent phases (all results at the B3LYP-D3 level).

System	Phase	Zn	C5	O1	O2	Ti1	Ti2
LD14-TiO_2	Gas	1.576	0.843	−0.700	−0.663	1.510	1.526
	Solv	1.595	0.846	−0.717	−0.698	1.494	1.508
LD14	Gas	1.578	0.801	−0.708	−0.600		
	Solv	1.598	0.818	−0.717	−0.643		
TiO_2	Gas					1.544	1.605
	Solv					1.662	1.587

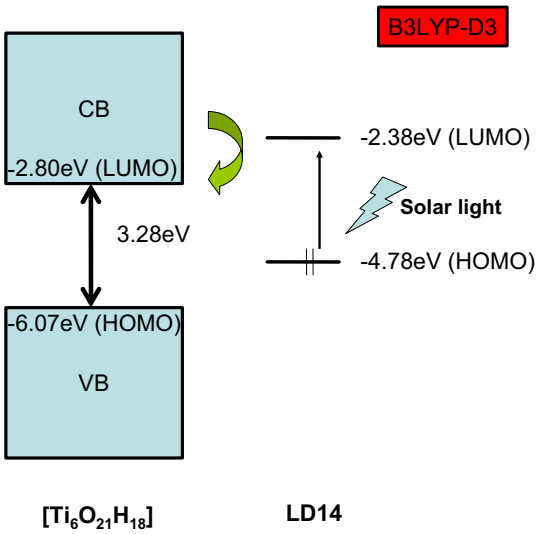

Fig. 3. Schematic energy level diagram of the absorption of solar light by LD14 and electron injection on TiO_2 cluster.

Table 5
Principal electronic transitions in LD14 and LD14–TiO_2. B and Q bands maxima (λ_{max}) in nm.

Method	B	Q
LD14 (B3LYP-D3)	417	597
LD14 (B3LYP-D3 (solv))	429	638
LD14 (PBE-D3)	457	824
LD14 (PBE-D3 (solv))	466	890
LD14-TiO_2 (B3LYP-D3)[a]	478	577
LD14-TiO_2 (B3LYP-D3 (solv))[a]	416	614
LD14 Exp[b] [24]	459	667
LD14-TiO_2 Exp[b] [24]	464	663

[a] $[Ti_6O_{21}H_{18}]$ cluster of TiO_2.
[b] THF.

such as TPP–Zn(II)–TiO_2, which are between 56.0 and 47.0 kcal mol^{-1} [38].

On the other hand, we carried out a Natural Population Analysis (NPA) at the B3LYP-D3 level with the LD14, TiO_2 and LD14–TiO_2 models in the gas and solvent phases. The results are summarized in Table 4 for some selected atoms. In general, a charge transfer of 0.113e and 0.247e in the gas and solvent phases may be noticed, respectively, from the LD14 to the surface of TiO_2. This is noticeable from the values in Table 4, which show that the charge on the oxygen atoms for LD14 decreases when the molecule is anchored to the TiO_2. Therefore, the charge on the Ti atoms in TiO_2 increases when the LD14 is adsorbed. The carbon atom in the anchor group is more positive and the Zn atom in the porphyrin does not substantially change its charge.

3.2. Time-dependent (TD) DFT calculations for YD2 and YD2–TiO_2

As mentioned in Models and Computational Details section, we used the B3LYP, PBE and TPSS functionals with dispersion correction (D3); but finally we adopted the B3LYP functional in the electronic absorption process because it is the only functional able to correctly describe the process of injection of charge from the LD14 to TiO_2, as shown in Fig. 3.

TD-DFT has proved to be an important tool for studying the optical properties of LD14 in DSSCs. The LD14–TiO_2 electronic coupling determines the electron injection rate, and therefore the conversion index (η), which involves properties that are directly related to the excited states. Thus, it is necessary to describe the properties of the excited states of the LD14 and LD14–TiO_2. For porphyrins, the UV–Vis absorption spectrum in the visible region usually shows a Q band, a weak T band, and a B (or Soret) band at higher energy. The calculated absorption excitation energies for LD14 and LD14–TiO_2 are reported in Table 5 for the Q and B bands. The studied system shows the Q band in the region between 890 nm and 577 nm, and the B band at around 460 nm. In the PBE-D3 method, the Q band is overestimated for both LD14 and LD14–

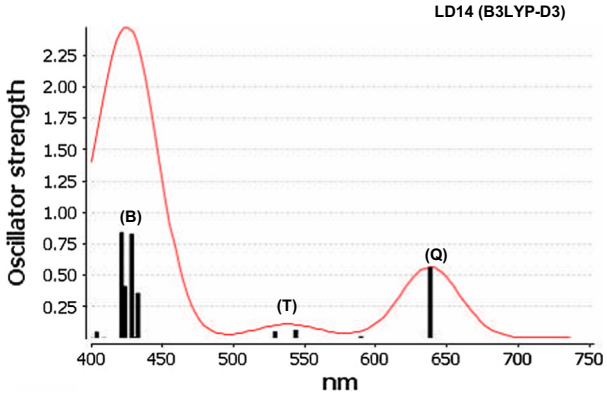

Fig. 4. Calculated B3LYP-D3 electronic spectra of LD14 in solvent.

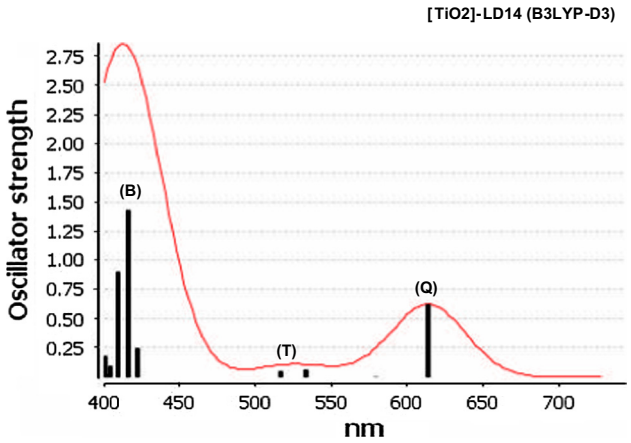

Fig. 6. Most important active molecular orbitals in the electronic transitions of LD14 models at the B3LYP-D3 level in solvent.

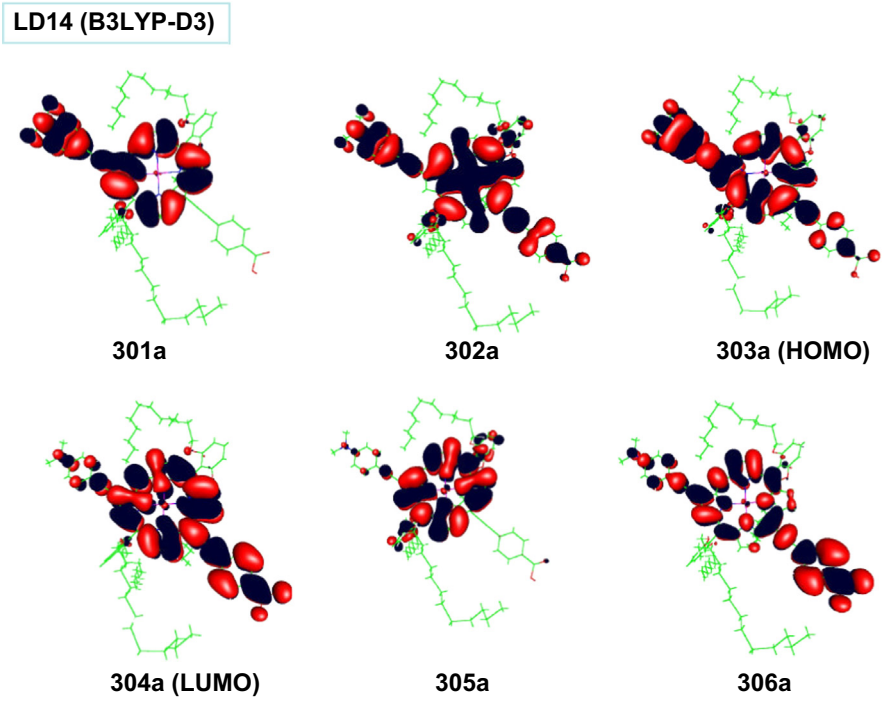

Fig. 5. Calculated B3LYP-D3 electronic spectra of LD14–TiO_2 in solvent.

TiO_2 models. The data indicate that the most accurate functional for the B and Q bands is B3LYP-D3 when we compare these obtained values against their experimental UV–Vis absorption spectra [24]. So the B3LYP-D3 functional is used to describe the excited states of the LD14 and LD14–TiO_2 models described below.

Oscillator strengths different from zero were considered as allowed transitions. The allowed transitions obtained at the B3LYP-D3 level are shown in Figs. 4 and 5 for LD14 and LD14–TiO_2 in the solvent phase (THF), respectively. The active molecular orbitals in the electronic transitions are shown in Figs. 6 and 7 for LD14 and LD14–TiO_2, respectively. We do notice that the experimental spectra show a small shoulder between 550 and 600 nm [24]. This is in agreement with the weak T band described in the theoretical spectra (Figs. 4 and 6).

3.2.1. LD14

The electronic structure of this model is described with the three absorption peaks which were mentioned above. The electronic transitions are assigned to individual states as ligand-to-ligand, metal–ligand-to-ligand and ligand-to-ligand–metal charge transfer (LLCT, MLLCT and LLMCT), respectively. The theoretical calculations are described in Table 6 showing good agreement with the experimental results [24]. The bands are a mixture of excitations. Band Q is formed by the transition at 638 nm. This transition is mainly composed of 303a → 304a ($\pi^* \rightarrow \pi^*$) (HOMO–LUMO). This band corresponds to LLCT. The frontier MOs are shown in Fig. 5. The 303a (HOMO) has a porphyrin π^* character, while the arrival orbital 304a (LUMO) shows a main composition centered on the porphyrin and phenylethynyl carboxylic acid. Both orbitals have a π^* character while the Zn atom shows a small contribution.

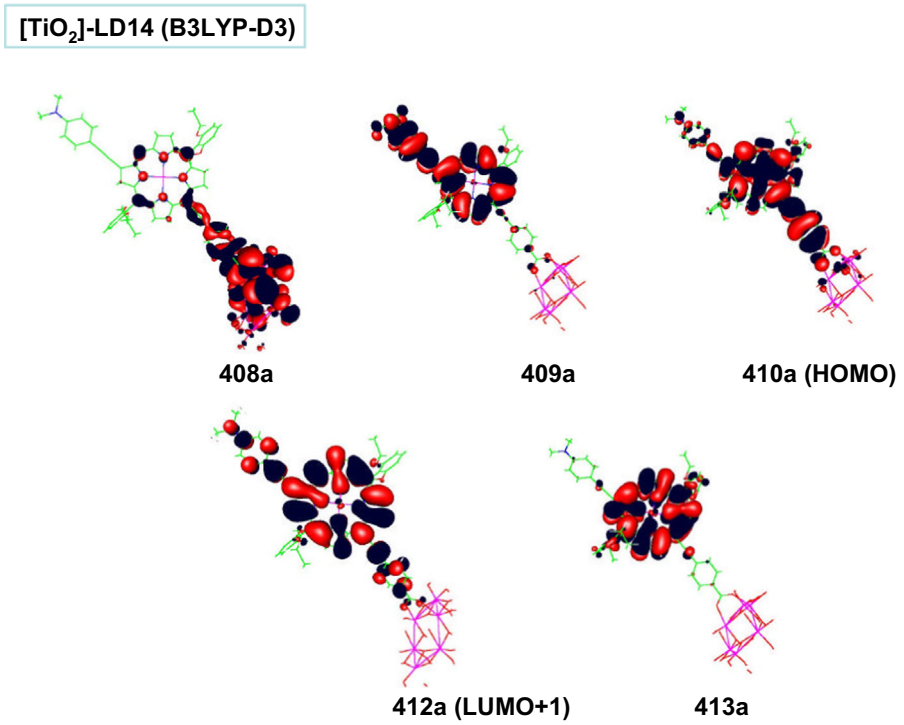

Fig. 7. Most important active molecular orbitals in the electronic transitions of LD14–TiO_2 models at the B3LYP-D3 level in solvent.

Table 6
TD-DFT/B3LYP-D3 singlet-excitation calculations for LD14 and LD14-TiO_2 in solvent.

System	λ_{calc}	λ_{exp}	f[a]	Contribution[b]	Transition type
LD14	638 (**Q**)	667	0.564	303a → 304a (83%)	LLCT ($\pi^* \rightarrow \pi^*$)
	529 (**T**)		0.052	303a → 305a (39%)	LLMCT ($\pi^* \rightarrow \pi^* + d_{xz}$)
				302a → 305a (26%)	MLLMCT ($d_{zx}/d_{zy} + \pi^* \rightarrow \pi^* + d_{xz}$)
	429 (**B**)	459	0.832	303a → 306a (48%)	LLMCT ($\pi^* \rightarrow \pi^* + d_{yz}$)
				301a → 304a (40%)	LLCT ($\pi^* \rightarrow \pi^*$)
	422 (**B**)		0.845	301a → 305a (60%)	LLMCT ($\pi^* \rightarrow \pi^* + d_{xz}$)
				302a → 306a (38%)	MLLCT ($d_{zx}/d_{zy} + \pi^* \rightarrow \pi^*$)
LD14-TiO_2	614 (**Q**)	663	0.625	410a → 412a (65%)	MLLCT ($d_{zx}/d_{zy} + \pi^* \rightarrow \pi^*$)
				409a → 413a (15%)	LLCT ($\pi^* \rightarrow \pi^*$)
	517 (**T**)		0.053	409a → 412a (23%)	LLCT ($\pi^* \rightarrow \pi^*$)
				409a → 413a (23%)	LLCT ($\pi^* \rightarrow \pi^*$)
				408a → 412a (13%)	MLCT ($d_{Ti} \rightarrow \pi^*$)
	416 (**B**)	464	1.433	409a → 413a (25%)	LLCT ($\pi^* \rightarrow \pi^*$)
				409a → 412a (22%)	LLCT ($\pi^* \rightarrow \pi^*$)
				408a → 412a (17%)	MLCT ($d_{Ti} \rightarrow \pi^*$)
				410a → 413a (13%)	MLLCT ($d_{zx}/d_{zy} + \pi^* \rightarrow \pi^*$)

[a] Oscillator strength.
[b] Values are |coeff.|$^2 \times 100$.

The T band is formed by a transition at 529 nm, and it shows a principal component 303a → 305a ($\pi^* \rightarrow \pi^*$) of the LLMCT type. We must point out that the 303a orbital corresponds to a π^* orbital of the porphyrin ring. Thus, in the transition involved this orbital goes to the 305a orbital, which is centered mainly on the porphyrin and a small contribution from the d_{xz} orbital of Zn. The experimental spectra show a small shoulder between 550 and 600 nm [24], which is comparable with the theoretical bandwidth.

Finally, the B band is formed by two transitions, the one at 429 nm is composed mainly of 303a → 306a ($\pi^* \rightarrow \pi^* + d_{yz}$) of the LLMCT type. The 303a (HOMO) has been described above, while the 306a MO (LUMO + 2) contains a principal contribution of phenylethynyl carboxylic acid with porphyrin and a small contribution from the d_{yz} orbital of Zn. The second transition at 422 nm has a principal 301a → 305a ($\pi^* \rightarrow \pi^* + d_{xz}$) excitation which is associated with LLMCT.

3.2.2. YD2–TiO_2

When the LD14–TiO_2 model was used, a shift of the excited bands compared with free LD14 is observed (see Table 6). This shift also occurs at an experimental level when going from the dye in solution to the one deposited on TiO_2. There is good agreement with the experimental results and the change of the spectrum once LD14 is attached to TiO_2 (Fig. 6). The principal bands of the LD14 dye on TiO_2 are maintained. The Q band (614 nm) is built by a main transition between HOMO and LUMO + 2 of LD14: 410a → 412a ($d_{zx}/d_{zy} + \pi^* \rightarrow \pi^*$) associated with MLLCT. The 410a (HOMO) has a porphyrin π^* character, Zn orbitals, and contribution of phenylethynyl carboxylic acid, while the arrival orbitals 412a (LUMO + 1) show a main composition centered on the porphyrin and phenylethynyl carboxylic acid. The frontier MOs are shown in Fig. 7.

The very weak T band (547 nm) is composed of several transitions, which are described in Table 6. Finally, the last band (B) at 416 nm is formed by several transitions. There are two main transitions: 409a → 413a ($\pi^* \rightarrow \pi^*$) transition of the LLCT type. Both orbitals have a π^* orbital of the porphyrin ring. The second transition is among 409a → 412a ($\pi^* \rightarrow \pi^*$) excitation which is associated with LLCT.

3.3. Absorption properties

The photo-induced electron injection in DSSCs can be viewed as a charge transfer (CT) process [41,42,54]. Using the Marcus theory for electron transfer [55], the CT can be associated with the free energy change for electron injection (ΔG^{inject}) [56]. ΔG^{inject} is a measure of the electron injection rate and therefore the short-circuit current density (J_{sc}) and open-circuit (V_{oc}) in DSSCs. In general, the greater the ΔG^{inject}, the greater the electron-injection efficiency (Φ^{inject}). It can be calculated as $\Delta G^{inject} = E^{dye*} - E_{CB}$ [57]. E_{CB} is the reduction potential of the conduction band of the TiO_2, which has an experimental value of −4.00 eV (widely used) [58]. E^{dye*} is the excited state oxidation potential of the dye, and it is determined by the redox potential of the ground state of the dye (E^{dye}), and the vertical transition energy (λ_{max}): $E^{dye*} = E^{dye} - \lambda_{max}$. The E^{dye} is calculated by two approaches: a first level, applying molecular orbitals eigenvalues on the basis of Koopmans' theorem as IP ≈ $-E_{HOMO}$ [59]. This is accepted in the literature within the framework of the Conceptual Density Functional Theory (CDFT) [60,61]. A second level, the energy of the orbital that generates the transition in the band. The calculated E^{dye*} and ΔG^{inject} of the Q and B bands for LD14 dye in solvent phase are listed in Table 7.

The calculated E^{dye*} of the Q and B bands used the energy of the orbital generate from transition in the band and HOMO energy are same. This is because it is the same orbital involved in the calculation. On the other hand, when the experimental value of E_{CB} (−4.0 eV) was used, the values of ΔG^{inject} of the LD14 are negative, which means that the LD14 excited state with effective charge transfer excitation character lies above the TiO_2 conduction band edge. The large absolute value of the free energy for electron injection is favourable for fast electron injection and it is directly proportional to the experimental values of J_{SC} and V_{OC}. However, if a theoretical value of the E_{CB} as LUMO of the TiO_2 cluster is used, only some values of ΔG^{inject} are negative by Q band. This shows that the proposed cluster model is only an approximation and it is necessary to build larger systems.

Table 7
The calculated excited state oxidized potential (E^{dye*}/eV) and free energy change for electron injection (ΔG^{inject}/eV) of the Q and B absorption bands for LD14 in solvent phase at the B3LYP-D3 level. E_{CB} is used with an experimental value of −4.00 eV; the value in parentheses is taken from the LUMO value of the TiO_2 cluster.

Phase	E^{dye*}		ΔG^{inject}	
	Q	**B**	**Q**	**B**
Solvent[a]	2.7	1.89	−1.3 (−0.09)	−2.1 (0.1)
Solvent[b]	2.7	1.89	−1.3 (−0.09)	−2.1 (0.1)

[a] E^{dye} is the energy of the orbital that generates the transition in the band.
[b] E^{dye} is the absolute value of the HOMO energy.

4. Conclusions

The present study of the electronic structures and spectroscopic properties of the dye LD14 free and adsorbed on TiO_2 clusters provide further support to the idea that the DSSCs is a supramolecular structure strengthened by ligand anchoring to the electrode. The calculated geometric parameters are very similar and in very good agreement despite the different methods used in both gas and solvent phases. The coordination energy between the —COO^- anchor group and TiO_2 lies between 45 and 50 kcal mol^{-1} depending on the calculation level, showing the importance of incorporating dispersion effects. The charge transfer analysis shows that LD14 injects electrons to the TiO_2 cluster. Such a transfer is more pronounced in the solvent phase. The obtained spectra at the B3LYP-D3 TD-DFT level demonstrate that this is the most suitable functional for describing the Q and B bands of porphyrins in the LD14 free and LD14–TiO_2 models. The absorption energy is centered on the LD14. The LUMO of the dye is delocalized in the region of the TiO_2 cluster conduction band. MO analysis supports the idea that the diarylamino groups are major ligands for electronic charge and act as electron donors in photon-induced electron injection in DSSCs. Using the Marcus theory for electron transfer, the CT can be associated with the free energy change for electron injection (ΔG^{inject}): i.e. LD14 and LD14–TiO_2 models show a large absolute value.

Acknowledgements

Financial support of this work under Conicyt-Aka-ERNC-001, Fondecyt 1140503 and 1150629, Project RC120001 of the Iniciativa Científica Milenio (ICM) del Ministerio de Economía, Fomento y Turismo del Gobierno de Chile. We are gratefully appreciated.

References

[1] K.S. Gallagher, Why & how governments support renewable energy, Daedalus 142 (2013) 59–77.
[2] G.K. Singh, Solar power generation by PV (photovoltaic) technology: a review, Energy 53 (2013) 1–350.

[3] B. O'Regan, M. Grätzel, A low-cost, high-efficiency solar cell based on dye-sensitized colloidal TiO_2 films, Nature 353 (1991) 737–740.
[4] M. Grätzel, Recent advances in sensitized mesoscopic solar cells, Acc. Chem. Res. 42 (2009) 1788–1798.
[5] A. Hagfeldt, G. Boschloo, L. Sun, L. Kloo, H. Pettersson, Dye-sensitized solar cells, Chem. Rev. 110 (2010) 6595–6663.
[6] M. Urbani, M. Grätzel, M.K. Nazeeruddin, T. Torres, Meso-substituted porphyrins for dye-sensitized solar cells, Chem. Rev. 114 (2014) 12330–12396.
[7] H. Imahori, T. Umeyama, S. Ito, Large π-aromatic molecules as potential sensitizers for highly efficient dye-sensitized solar cells, Acc. Chem. Res. 42 (2009) 1809–1818.
[8] M. Pastore, E. Mosconi, F. De Angelis, M. Grätzel, A computational investigation of organic dyes for dye-sensitized solar cells: benchmark, strategies, and open issues, J. Phys. Chem. C 114 (2010) 7205–7212.
[9] F. De Angelis, S. Fantacci, E. Mosconi, M.K. Nazeeruddin, M. Grätzel, Absorption spectra and excited state energy levels of the N719 dye on TiO_2 in dye-sensitized solar cell models, J. Phys. Chem. C 115 (2011) 8825–8831.
[10] F. Gajardo, M. Barrera, R. Vargas, I. Crivelli, B. Loeb, Influence of the nature of the absorption band on the potential performance of high molar extinction coefficient ruthenium(II) polypyridinic complexes as dyes for sensitized solar cells, Inorg. Chem. 50 (2011) 5910–5924.
[11] F. Gajardo, A. Leiva, B. Loeb, A. Delgadillo, J. Stromberg, G. Meyer, Interfacial electron transfer on TiO_2 sensitized with an axially anchored trans tetradentate Ru (II) compound, Inorg. J. Chim. Acta 361 (2008) 613–619.
[12] M. Pastore, S. Fantacci, F. De Angelis, Modeling excited states and alignment of energy levels in dye-sensitized solar cells: successes, failures, and challenges, J. Phys. Chem. C 117 (2013) 3685–3700.
[13] D. Casanova, F.P. Rotzinger, M. Grätzel, Computational study of promising organic dyes for high-performance sensitized solar cells, J. Chem. Theory Comput. 6 (2010) 1219–1227.
[14] J. Feng, Y. Jiao, W. Ma, M.K. Nazeeruddin, M. Grätzel, S. Meng, First principles design of dye molecules with ullazine donor for dye sensitized solar cells, J. Phys. Chem. C 117 (2013) 3772–3778.
[15] J. Warnan, Y. Pellegrin, E. Blart, F. Odobel, Supramolecular light harvesting antennas to enhance absorption cross-section in dye-sensitized solar cells, Chem. Commun. 48 (2012) 675–677.
[16] A. Yella, H.W. Lee, H.N. Tsea, C.Y. Yi, A.K. Chandirian, M.K. Nazeeruddin, E.W.G. Diau, C.Y. Yeh, S.M. Zakeeruddin, M. Grätzet, Porphyrin-sensitized solar cells with cobalt (II/III)–based redox electrolyte exceed 12 percent efficiency, Science 334 (2011) 629–634.
[17] Y. Chang, C. Wang, Y.-T. Pan, H. Kuo, C. Lo, H. Hsu, C. Lin, E.W.-G. Diau, A strategy to design highly efficient porphyrin sensitizers for dye-sensitized solar cells, Chem. Commun. 47 (2011) 8910–8912.
[18] N.K. Subbaiyan, J.P. Hill, K. Ariga, S. Fukuzumi, F. DSouza, Enhanced photocurrents via redox modulation by fluoride binding to oxoporphyrinogen in a zinc porphyrin-oxoporphyrinogen surface modified TiO_2 supramolecular solar cell, Chem. Commun. 47 (2011) 6003–6005.
[19] T. Bessho, S.M. Zakeeruddin, C.-Y. Yeh, E.W.-G. Diau, M. Grätzel, Highly efficient mesoscopic dye-sensitized solar cells based on donor–acceptor-substituted porphyrins, Angew. Chem. Int. Ed. 49 (2010) 6646–6649.
[20] F. Silvestri, I. López, W. Seitz, M. Martínez, T.J. Marks, D. Guldi, T. Torres, A squaraine-phthalocyanine ensemble: towards molecular panchromatic sensitizers in solar cells, Chem. Commun. 45 (2009) 4500–4504.
[21] H.-P. Lu, C.-Y. Tsai, W.-N. Yen, C. Hsieh, C.-W. Lee, C.-Y. Yeh, E. Diau, Control of dye aggregation and electron injection for highly efficient porphyrin sensitizers adsorbed on semiconductor films with varying ratios of coadsorbate, J. Chem. Phys. C 113 (2009) 20990–20997.
[22] L.-L. Li, W.W.-G. Eiau, Porphyrin-sensitized solar cells, Chem. Soc. Rev. 42 (2013) 291–304.
[23] K. Kurotobi, Y. Toude, K. Kawamoto, Y. Fujimori, S. Ita, P. Chabera, V. Sundström, H. Imahori, Highly asymmetrical porphyrins with enhanced push-pull character for dye-sensitized solar cells, Chem. Eur. J. 19 (2013) 17075–17081.
[24] C.-L. Wang, C.-M. Lan, S.-H. Hong, Y.-F. Wang, T.-Y Pan, C.-W. Chang, H.-H. Kuo, M.-Y. Kuo, E.W.-G. Diau, C.-Y. Lin, Enveloping porphyrins for efficient dye-sensitized solar cells, Energy Environ. Sci. 5 (2012) 6933–6940.
[25] S. Liu, H. Fu, Y. Cheng, S. Wu, S. Ho, Y. Chi, P. Chou, Theoretical study of N749 dyes anchoring on the $(TiO_2)_{28}$ surface in DSSCs and their electronic absorption properties, J. Phys. Chem. C 116 (2012) 16338–16345.
[26] H. Kusama, K. Sayama, Theoretical study on the intermolecular interactions of black dye dimers and black dye-deoxycholic acid complexes in dye-sensitized solar cells, J. Phys. Chem. C 116 (2012) 23906–23914.
[27] F. De Angelis, S. Fantacci, A. Selloni, M.K. Nazeeruddin, M. Grätzel, First-principles modeling of the adsorption geometry and electronic structure of Ru (II) dyes on extended TiO_2 substrates for dye-sensitized solar cell applications, J. Phys. Chem. C 114 (2010) 6054–6061.
[28] E. Jakubikova, R.C. Snoeberger, V.S. Batista, R.L. Martin, E.R. Batista, Interfacial electron transfer in tio_2 surfaces sensitized with Ru(II)–polypyridine complexes, J. Phys. Chem. A 113 (2009) 12532–15540.
[29] T. Le Bahers, T. Pauporté, P.P. Lainé, F. Labat, C. Adamo, I. Ciofini, Modeling dye-sensitized solar cells: from theory to experiment, J. Phys. Chem. Lett. 4 (2013) 1044–1050.
[30] F. Risplendi, G. Cicero, G. Mallia, N.H. Harrison, A quantum-mechanical study of the adsorption of prototype dye molecules on rutile–TiO_2 (110): a comparison between catechol and isonicotinic acid, Phys. Chem. Chem. Phys. 15 (2013) 235–243.
[31] X. Zarate, E. Schott, T. Gomez, R. Arratía-Pérez, Theoretical study of sensitizer candidates for dye-sensitized solar cells: peripheral substituted dizinc pyrazinoporphyrazine–phthalocyanine complexes, J. Phys. Chem. A 117 (2013) 430–438.
[32] E. Mosconi, J. Yum, C. Gómez, M. Nazeeruddin, M. Grätzel, F. De Angelis, Cobalt electrolyte/dye interactions in dye-sensitized solar cells: a combined computational and experimental study, J. Am. Chem. Soc. 134 (2012) 19438–19453.
[33] E. Maggio, N. Martsinovich, A. Troisi, Evaluating charge recombination rate in dye-sensitized solar cells from electronic structure calculations, J. Phys. Chem. C 116 (2012) 7638–7649.
[34] L. Yang, L. Guo, Q. Chen, H. Yan, Q. Zeng, X. Zhang, X. Pan, S. Dai, Substituent effects on zinc phthalocyanine derivatives: a theoretical calculation and screening of sensitizer candidates for dye-sensitized solar cells, J. Mol. Graph. Mod. 38 (2012) 82–90.
[35] S. Grimme, J. Antony, S. Ehrlich, H. Krieg, A consistent and accurate ab initio parametrization of density functional dispersion correction DFT-D for the 94 elements H-Pu, J. Chem. Phys. 132 (2010) 154104–154112.
[36] W. Hujo, S. Grimme, Performance of the van der Waals density functional VV10 and (hybrid) GGA variants for thermochemistry and noncovalent interactions, J. Chem. Theor. Comput. 7 (2011) 3866–3871.
[37] K. Syres, A. Thomas, F. Bondino, M. Malvestuto, M. Grätzel, Dopamine adsorption on anatase TiO_2(101): a photoemission and NEXAFS spectroscopy study, Langmuir 26 (2010) 14548–14555.
[38] T. Gomez, X. Zarate, E. Schott, R. Arratia-Perez, Role of the main adsorption modes in the interaction of the dye [COOH–TPP–Zn (ii)] on a periodic TiO2 slab exposing a rutile (110) surface in a dye-sentized solar cell, RSC Adv. 4 (2014) 9639–9646.
[39] K.B. Ornso, C.S. Peterson, J.M. Garcia-Lastra, K.S. Thygesen, Optimizing porphyrins for dye sensitized solar cells using large-scale ab initio calculations, Phys. Chem. Chem. Phys. 16 (2014) 16246–16254.
[40] K. Chaitanya, X.-H. Ju, B.M. Heron, Theoretical study on the light harvesting efficiency of zinc porphyrin sensitizers for DSSCs, RSC Adv. 4 (2014) 26621–26634.
[41] J. Chen, F.-Q. Bai, J. Wang, L. Hao, Z.-F. Xie, Q.-J. Pan, H.-X. Zhang, Theoretical studies on spectroscopic properties of ruthenium sensitizers absorbed to TiO_2 film surface with connection mode for DSSC, Dyes Pigm. 94 (2012) 459–468.
[42] J. Chen, J. Wang, F.-Q. Bai, L. Hao, Q.-J. Pan, H.-X. Zhang, Connection style and spectroscopic properties: theoretical understanding of the interface between N749 and TiO_2 in DSSCs, Dyes Pigm. 99 (2013) 201–208.
[43] M. Casida, in: D. Chong (Ed.), Recent Advances in Density Functional Methods (I), World Scientific, 1995, p. 155.
[44] M.E. Casida, C. Jamorski, K.C. Casida, D.R. Salahub, Molecular excitation energies to high-lying bound states from timedependent density-functional response theory: Characterization and correction of the time-dependent local density approximation ionization threshold, J. Chem. Phys. 108 (1998) 4439–4449.
[45] R. Bauernschmitt, R. Ahlrichs, Treatment of electronic excitations within the adiabatic approximation of time dependent density functional theory, Chem. Phys. Lett. 256 (1996) 454–464.
[46] P. Deglmen, F. Furche, R. Ahlrichs, An efficient implementation of second analytical derivatives for density functional methods, Chem. Phys. Lett. 362 (2002) 511–518.
[47] Turbomole: ab initio program, R. Ahlrichs, M. Bär, M. Häser, H. Horn, C. Kölmel, Electronic structure calculations on workstation computers: The program system turbomole, Chem. Phys. Lett. 162 (1989) 165–169.
[48] A. Klamt, G. Schüürman, COSMO: a new approach to dielectric screening in solvents with explicit expressions for the screening energy and its gradient, J. Chem. Soc. Perkin Trans. 5 (1993) 799–805.
[49] D. Andrae, U. Haeussermann, M. Dolg, H. Stoll, H. Preuss, Energy-adjusted ab initio pseudopotentials for the second and third row transition elements, Theor. Chim. Acta 77 (1990) 123–141.
[50] A. Bergner, M. Dolg, W. Küchle, H. Stoll, H. Preuss, Ab initio energy-adjusted pseudopotentials for elements of groups 13–17, Mol. Phys. 80 (1993) 1431–1441.
[51] T. Dunning, P. Hay, in: H. Schaefer (Ed.), Modern Theoretical Chemistry, 3, Plenum Press, 1997, pp. 1–28.
[52] S. Huzinaga, Gaussian-type functions for polyatomic systems. I, J. Chem. Phys. 52 (1965) 1293–1301.
[53] K. Eichkorn, O. Treutler, H. Öhm, M. Häser, R. Ahlrichs, Auxiliary basis sets to approximate Coulomb potentials, Chem. Phys. Lett. 240 (1995) 283–289.
[54] L.-H. Han, C.-R. Zhang, J.W. Zhe, N.-Z. Jin, Y.-L. Shen, W. Wang, J.J. Gong, Y.-H. Chen, Z.-J. Liu, Understanding the electronic structures and absorption properties of porphyrin sensitizers YD2 and YD2-o-C8 for dye-sensitized solar cells, Int. J. Mol. Sci. 14 (2013) 20171–20188.
[55] R.A. Marcus, Electron transfer reactions in chemistry. Theory and experiment, Rev. Mod. Phys. 65 (1993) 599–610.
[56] W. Fan, D. Tan, W.-Q. Deng, Acene modified triphenylamine dyes for dye-sensitized solar cells: a computational study, ChemPhysChem 13 (2012) 2051–2060.
[57] J. Preat, C. Michaux, D. Jacquemin, E.A. Perpete, Enhanced efficiency of organic dye-sensitized solar cells: triphenylamine derivatives, J. Phys. Chem. C 113 (2009) 16821–16833.
[58] J.B. Asbury, Y.-Q. Wang, E. Hao, H.N. Ghosh, T. Lian, Evidences of hot excited state electron injection from sensitizer molecules to TiO_2 nanocrystalline thin films, Res. Chem. Intermed. 27 (2001) 393–406.

[59] T. Koopmans, Uber die Zuordnung von Wellenfunktionen und Eigenwerten zu den einzelnen Elektronen eines Atoms, Physica 1 (1934) 104–113.
[60] P. Geerlings, F. De Proft, W. Langenaeker, Conceptual density functional theory, Chem. Rev. 103 (2003) 1793–1874.
[61] M. Torrent-Sucarrat, F. De Proft, P. Geerlings, P.W. Ayers, Do the local softness and hardness indicate the softest and hardest regions of a molecule?, Chem Eur. J. 14 (2008) 8652–8660.